

See discussions, stats, and author profiles for this publication at: <https://www.researchgate.net/publication/308171670>

# Optimization and experimental verification of coplanar interdigital electroadhesives

Article in *Journal of Physics D Applied Physics* · September 2016

DOI: 10.1088/0022-3727/49/41/415304

---

CITATIONS  
47

READS  
5,697

---

3 authors:



Jianglong Guo  
Harbin Institute of Technology (Shenzhen)

40 PUBLICATIONS 484 CITATIONS

[SEE PROFILE](#)



Tom Bamber  
Loughborough University

9 PUBLICATIONS 159 CITATIONS

[SEE PROFILE](#)



Matthew R Chamberlain  
Loughborough University

6 PUBLICATIONS 142 CITATIONS

[SEE PROFILE](#)

Some of the authors of this publication are also working on these related projects:



Intelligent Handling [View project](#)



Unmanned Vehicles [View project](#)

## Optimization and experimental verification of coplanar interdigital electroadhesives

This content has been downloaded from IOPscience. Please scroll down to see the full text.

2016 J. Phys. D: Appl. Phys. 49 415304

(<http://iopscience.iop.org/0022-3727/49/41/415304>)

View the [table of contents for this issue](#), or go to the [journal homepage](#) for more

Download details:

IP Address: 86.17.184.213

This content was downloaded on 16/09/2016 at 16:45

Please note that [terms and conditions apply](#).

# Optimization and experimental verification of coplanar interdigital electroadhesives

J Guo<sup>1</sup>, T Bamber, M Chamberlain, L Justham and M Jackson

EPSRC Centre for Innovative Manufacturing in Intelligent Automation, Loughborough University,  
Loughborough, UK

E-mail: [J.Guo@lboro.ac.uk](mailto:J.Guo@lboro.ac.uk)

Received 3 June 2016, revised 14 August 2016

Accepted for publication 1 September 2016

Published 16 September 2016



CrossMark

## Abstract

A simplified and novel theoretical model for coplanar interdigital electroadhesives has been presented in this paper. The model has been verified based on a mechatronic and reconfigurable testing platform, and a repeatable testing procedure. The theoretical results have shown that, for interdigital electroadhesive pads to achieve the maximum electroadhesive forces on non-conductive substrates, there is an optimum electrode width/space between electrodes (width/space) ratio, approximately 1.8. On conductive substrates, however, the width/space ratio should be as large as possible. The 2D electrostatic simulation results have shown that, the optimum ratio is significantly affected by the existence of the air gap and substrate thickness variation. A novel analysis of the force between the electroadhesive pad and the substrate has highlighted the inappropriateness to derive the normal forces by the division of the measured shear forces and the friction coefficients. In addition, the electroadhesive forces obtained in a 5 d period in an ambient environment have highlighted the importance of controlling the environment when testing the pads to validate the models. Based on the confident experimental platform and procedure, the results obtained have validated the theoretical results. The results are useful insights for the investigation into environmentally stable and optimized electroadhesives.

Keywords: electroadhesion, experimental validation, interdigital electroadhesive, optimization modelling

(Some figures may appear in colour only in the online journal)

## 1. Introduction

Electroadhesion is an electrostatic attractive effect between the electroadhesive pad and the substrate [1]. Electroadhesion has been extensively used for many applications. This includes: electrostatic fixtures to hold workpieces [2], an adhesive method for space missions such as material handling [3] and controllable earth orbit grappling [4], electrostatic chucks for material handling and grasping in semiconductor industries [5], end effectors for gripping advanced composites

and fibrous materials such as cloth [6] and carbon fibres [7, 8], an adhesion mechanism for robots [9–11], and material handling units for manufacturing automation and warehouse automation [12]. This is because, compared with other adhesion mechanisms [13],

- Electroadhesion has an enhanced adaptability as it adheres to both conductive and insulating materials such as smooth aluminium and rough concrete surfaces [14]. In addition, it can be applied in a vacuum, and therefore, space environments [3, 4]. Vacuum environments are also increasingly desirable for high-value chip manufacturers [15].
- Electroadhesive grasping is a gentle material handling method as it can be applied without contact with the substrates [16], so it is non-damaging or less-damaging to the substrate surface, which is desirable for some high value

<sup>1</sup> Author to whom any correspondence should be addressed.

Original content from this work may be used under the terms of the [Creative Commons Attribution 3.0 licence](#). Any further distribution of this work must maintain attribution to the author(s) and the title of the work, journal citation and DOI.

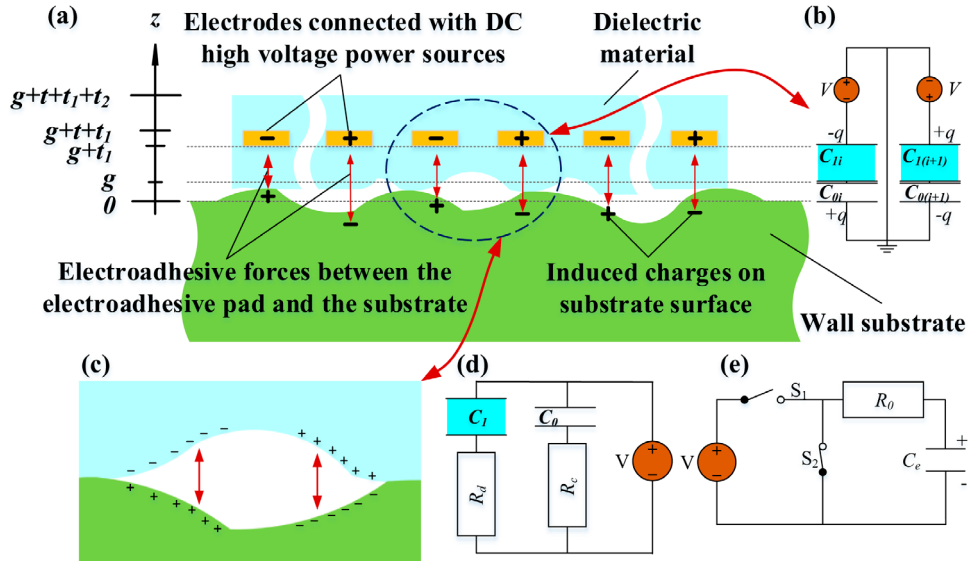


**Figure 1.** Principle of electroadhesion on conductive and semi-conductive substrates: (a) is the cross sectional view of the electroadhesive system, (b) is the equivalent circuit of two adjacent electrodes in series, (c) is charges accumulated between the non-contact areas [35], (d) is the equivalent circuit of the J-R type electroadhesive [35], and (e) is the equivalent circuit of the Coulomb type electroadhesive [36].

material handling tasks such as pick-and-place of silicon wafers in the semiconductor industries [15].

- Furthermore, electroadhesion can bring lightweight and reduced complexity systems as it can help reduce the weight and complexity of a system in terms of control and the mechanical structure as it enables electrically controllable clamping and unclamping, which means pumps or motors are not required.
- Last but not the least, electroadhesion is an ultra-low energy consumption adhesion method (usually in the  $\mu\text{W}$  to  $\text{mW}$  range) as a very small current in the  $\mu\text{A}$  to  $\text{mA}$  range runs through the electroadhesive pad [17]. This feature helps to reduce the energy consumed in pick-and-place applications by up to three orders of magnitude [12, 18].

An electroadhesion system contains four essential components: the electroadhesive pad, the substrate the pad to be adhered onto, the high voltage power supply to energize the pad, and the control system. The electroadhesive pad contains conductive electrodes connected with high voltage power sources and embedded in dielectric materials, as seen in figure 1(a). The dielectric material serves as dielectric buffers, preventing the charge neutralization and dielectric breakdown. The dielectric material can be air, so bare electrodes can be used for electroadhesive grasping some non-conductive materials. Electroadhesion is a multidisciplinary, complicated, and dynamic electrostatic attraction phenomenon with over 33 variables influencing the electroadhesive forces obtainable between the electroadhesive pad and the substrate based on the literature survey [19]. These influencing factors include: (1) environmental factors such as ambient temperature, humidity, ambient pressure, contaminates, and the air pressure between the pad and substrate after applying the voltage, (2) electrode parameters such as electrode pattern, electrode width, space between electrodes, electrode thickness, electrode length, electrode thickness, conductivity, and effective electrode area, (3) pad dielectric parameters such as

dielectric resistivity, dielectric permittivity, dielectric strength, dielectric surface texture, dissipation factor, dielectric molecular structure, weight, and polarizability, crystallinity, electronegativity, and electropositivity, (4) substrate parameters such as substrate resistivity, permittivity, dielectric strength, thickness, surface texture, molecular structure, weight, and polarizability, crystallinity, electronegativity, and electropositivity, and (5) voltage parameters such as voltage polarity (positive/negative/zero), voltage magnitude, and voltage type (direct/alternating current) [19].

A recognized and cost-effective procedure to investigate a research phenomenon like electroadhesion commonly contains two steps: (1) theoretical modelling or computational simulation and (2) physical experiments to support the modelling results [1]. It is difficult or impossible to derive accurate analytical models to predict the theoretical electroadhesive forces due to inhomogenous materials and electric fields existing in nature. However, approximate or simplified modelling of electroadhesion based on assumptions is helpful for both understanding of the electroadhesion phenomenon and providing an idea of the scale of the electroadhesive forces obtainable. This can help guide the design, manufacture, testing, and application of electroadhesives.

Interdigital shape based sensors and transducers have been widely used both in research and industrial applications [20]. Interdigitated geometry has been one of the most popular designs for electroadhesive applications due to the fact that interdigitated electroadhesives can offer larger electroadhesive forces and quicker response times on insulating substrates [21]. Theoretical electroadhesive forces can generally be derived by the virtual work method [22] and Maxwell stress tensor method [23–25]. Simple theoretical models based on classic theories on parallel capacitors have been used by most researchers [26–29] to derive the electroadhesive forces. These models, however, usually do not include enough geometric information of the interdigital electroadhesives such as

electrode widths and spaces between electrodes. Also, there is a significant difference in the results of different publications. Although various theoretical models and electrostatic simulation models have been used, only the most recent theoretical model by Cao *et al* [30], the simulation model achieved by Ruffatto *et al* based on a gradient descent optimization algorithm coupled with COMSOL [31], the optimization model achieved by Koh *et al* based on an empirical comb capacitance equation [32], and the simulation model by Saberman *et al* based on COMSOL [33], concluded that there is an optimum electrode width for electroadhesive pads to achieve the maximum forces on insulating substrates when the space between the electrodes was fixed (i.e. an optimal width/space ratio). All the other theoretical and simulation models concluded that the smaller the electrode width, the larger the electroadhesive forces obtainable on non-conductive substrates. In addition, few researchers have experimentally validated their theoretical and simulation results due to the reason that it takes efforts, time and fund, to implement a repeatable pad design, manufacture, and testing platform, and conduct numerous experiments based on a confident and repeatable experiment procedure. Only the work by Ruffatto *et al* have validated some of their simulation results. However, the tests were not conducted in a controlled environment. In summary, there is little work on the experimental validation of the theoretical optimization modelling of interdigital electroadhesive actuators on both conductive substrates and non-conductive substrates.

A simplified and novel theoretical model for optimizing the design of coplanar interdigitated electroadhesives has been developed and validated in this paper. The basic principle of electroadhesion has been presented in section 2. The proposed optimization model for coplanar interdigitated electroadhesives, with a worked example, has been demonstrated in section 3. In order to further support the theoretical results, a 2D finite element analysis based electrostatic simulation has also been presented, as shown in section 4. Finally, in section 5, an experimental validation of the theoretical and simulation results has been conducted based on an advanced electroadhesive force measurement platform and procedure in a controlled environment, before the conclusions and future work summarized in section 6.

## 2. Principle and basic theoretical models of electroadhesion

The principle of the electroadhesive force generation on conductive and insulating substrate materials is different [26]. For conductive substrates, the electroadhesive forces are generated mainly by electrostatic induction. For insulating substrates, the electroadhesive forces are generated mainly by electric polarizations [31].

### 2.1. Electroadhesive forces on conductive substrates

The electrostatic induction phenomenon is a process where the formation of negative charges on one side and positive charges on the opposite side of a conductor are induced by the external electrostatic field produced by a charged insulator

[34]. Conducting materials generally refer to materials consisting of a large amount mobile free charge carriers. In a metal, the concentration of free electrons (mobile charge carriers) is of the same order as that of the number of atoms, i.e. about  $10^{22}$ – $10^{23}$  cm $^{-3}$  [34]. These electrons are able to rearrange themselves quickly and easily. Equal and opposite charges are induced on the surface of conductive substrates after the application of the high voltage on the electroadhesive pad. The electroadhesive forces between the pad and the conductive substrate are thus formed. When facing conductive substrate materials, dielectric materials with different properties such as the volume resistivity will cause different mechanisms of generating the electroadhesive forces. A volume resistivity over  $10^{14}$  Ω cm results in Coulomb type electroadhesive pads, whilst the volume resistivity between  $10^{10}$  and  $10^{12}$  Ω cm results in Johnsen–Rahbek (J–R) type pads. Both the Coulomb and J–R force will exist, to some degree, in all electroadhesive pads [35, 36].

The electroadhesive pad can be single-polar, bi-polar, and tri-polar [37]. The dual pole design has been the most frequently used design in electroadhesive applications. For the coulomb type dual-polar electroadhesive, the electroadhesive forces between the pad and substrate can be derived from a series of parallel connections of several ideal capacitors having dielectrics in series. The equivalent circuit of two adjacent electrodes in series from a multi-electrode and bi-polar electroadhesive during the electroadhesion operation can be seen in figure 1(b), where  $g$  is the effective air gap between the pad and the substrate,  $t_l$  is the dielectric thickness,  $C_{li}$  denotes the  $i$ th capacitance of the dielectric material, and  $C_{0i}$  denotes the  $i$ th capacitance of the air between the dielectric and the substrate surface. The total capacitance between the pad and substrate, therefore, can be given as

$$C_e = \sum_{i=1}^n \frac{C_{0i}C_{li}}{C_{0i} + C_{li}} = \frac{\varepsilon_0 \varepsilon_{rl} S}{\varepsilon_{rl} g + t_l}, \quad (1)$$

where  $n$  is the total number of capacitors in series or number of electrode pairs,  $S$  is the effective electroadhesive pad area,  $\varepsilon_0$  is the permittivity of the air, and  $\varepsilon_{rl}$  is the relative permittivity of the dielectrics.

Based on the virtual work method, the electroadhesive forces between the pad and the substrate can be given as

$$F_z = -\frac{1}{2} \frac{Q^2}{\varepsilon_0 S} = -\frac{1}{2} \frac{C_e^2 U^2}{\varepsilon_0 S}, \quad (2)$$

where  $U$  is the voltage potential,  $Q$  is the accumulated surface charge, and the negative sign corresponds to attractive forces.

The J–R effect [38], firstly investigated by Johnsen and Rahbek, occurs when attaching the electroadhesive pads made by attaching imperfect dielectrics with finite volume resistivity such as semi-conductive materials onto metal substrates. Current leakage or charge transfer will occur through the contacting points between the pads and the substrates. A strong electrostatic attractive force can be generated by the interfaces accumulated by charges between the non-contact areas, see figure 1(c). The comparably small gap is due to surface irregularities in nature, contributing to strong adhesion forces. Hence, for the J–R type electroadhesive, it is the potential difference

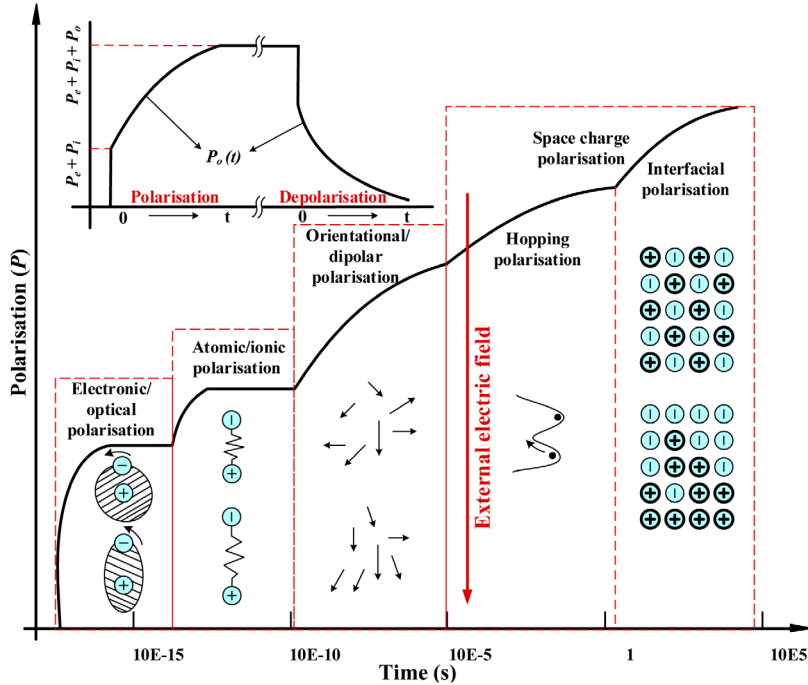


**Figure 2.** Polarization types of normal dielectric materials under a step-function electric field [34]. Reproduced with permission from [34]. Copyright 2004 Elsevier.

applied across the interfaces mentioned above, rather than that applied through the dielectric layer and the air gap, leading to the attractive forces. In this case, the J-R electrostatic attractive forces are independent from the dielectric material between the pad and the substrate [35], giving

$$F_{\text{J-R}} = -\frac{1}{2} \frac{C_0^2 V_{\text{J-R}}^2}{\varepsilon_0 S_{\text{J-R}}}, \quad (3)$$

where  $C_0 = \frac{\varepsilon_0 S_{\text{J-R}}}{g}$  is the capacitance of the non-contact areas,  $V_{\text{J-R}}$  is the potential difference across the interfaces, and  $S_{\text{J-R}}$  is the effective J-R non-contacting areas (usually assume to be the same as  $S$ ), subjected to the surface texture and attractive forces.

Based on the equivalent circuit of the J-R type electroadhesive shown in figure 1(d), the potential difference across the interfaces can be given as [35]

$$V_{\text{J-R}} = \frac{R_c}{R_c + R_d} U, \quad (4)$$

where  $R_d$  is the volume resistivity of the dielectric material and  $R_c$ , usually much larger than  $R_d$ , is the contact resistance subjected to surface texture, dielectric material property, and contacting areas.

Apart from the J-R electroadhesive forces, the conventional Coulomb forces will also be generated between the electrodes and the substrates, giving

$$F_z = F_{\text{Coulomb}} + F_{\text{J-R}} = -\frac{1}{2} \left( \frac{C_c^2 U^2}{\varepsilon_0 S} + \frac{C_0^2 V_{\text{J-R}}^2}{\varepsilon_0 S_{\text{J-R}}} \right). \quad (5)$$

$F_{\text{Coulomb}}$  is much smaller than  $F_{\text{J-R}}$  as the gap between the interfaces is usually much smaller than the thickness of the dielectric material, making  $F_{\text{Coulomb}}$  almost negligible. However, much shorter detachment times can be seen in the Coulomb type

electroadhesives [36]. Also, less current leakage occurs in coulomb type electroadhesives, resulting in significantly lower power consumption. With regard to the Coulomb type electroadhesive, the equivalent circuit can be seen in figure 1(e). When the switch  $S_1$  is on and  $S_2$  is off, the capacitance of the electroadhesive pad,  $C_e$ , is charged,  $Q$ , resulting in the attachment between the pad and the substrate. When the switch  $S_1$  is off and  $S_2$  is on ( $t = 0$ ), an exponentially decaying current will be demonstrated, described by [34]

$$I(t) = \frac{U}{R_0} \exp\left(-\frac{t}{\tau}\right), \quad (6)$$

where  $\tau = C_e R_0$  and  $R_0$  is the equivalent external resistance of the electroadhesive system.

The depolarization process, which involves a time period of bringing the excited system back to its original equilibrium state, can be referred to as dielectric relaxation. After switching off the voltage connected with the electrodes, i.e. removing the external electric field, the charge density decays with time and can be expressed as [29]

$$\sigma_s(t) = \sigma_s(0) e^{-t/\tau_d}, \quad (7)$$

where  $\tau_d = \rho_R \varepsilon$  is the dielectric relaxation time and the time needed for the originally induced charge to decay to 36.7% of its original value.

$\tau_d$  can be very large for some insulating materials [34]. However, (6) no longer applies in the J-R type electroadhesives. A non-exponentially decaying current will be shown, with much longer decrease time which is several orders of magnitude longer depending on the dielectric material property [36]. It is, therefore, necessary to balance the attraction forces and detachment time, tailoring to the specific requirements of tasks such as the pick and place of objects.

## 2.2. Electroadhesive forces on insulating substrates

The total polarization of an arbitrary dielectric system can be written as [15]

$$P_{\text{polarization}} = P_e + P_i + P_o + P_d + P_s + P_{\text{others}}, \quad (8)$$

where  $P_e$  is the electronic polarization,  $P_i$  is the ionic polarization,  $P_o$  is the orientational polarization,  $P_d = P_{\text{hop}} + P_{\text{face}}$  is the space charge polarization which includes the hopping polarization,  $P_{\text{hop}}$  and the interfacial polarization,  $P_{\text{face}}$ ,  $P_s$  is the spontaneous polarization, and  $P_{\text{others}}$  is other types of polarizations such as the nomadic polarization.

The approximate time required for each type of the mentioned polarization under a step function electric field  $E = \begin{cases} 0, & t = 0 \\ E, & t > 0 \end{cases}$  is shown in figure 2. The electroadhesive forces generated on insulating substrates can then be expressed by [31]

$$F_z = P_{\text{polarization}} E. \quad (9)$$

It was concluded by Monkman that electric polarizations, especially the orientational polarization and interfacial polarization, account for the generation of the electroadhesive forces [17]. This is, however, an assumption from Monkman and have not been experimentally validated with confidence. The electroadhesion phenomenon can also be contactless both on conductive substrates such as aluminium disks [39] and insulating substrates such as glass [16]. It was concluded by Jeon *et al* that the atomic and electric polarization account for the generation of the electroadhesive forces for contactless electroadhesive suspensions. The dynamic nature of the electroadhesion phenomenon manifests that the electrostatic adhesion force on a dielectric material will gradually increase to a steady value with some time. The steady value of the adhesion force is usually much larger than the initial value and the time period to reach the steady value is different. The experimental design and testing should therefore take this into consideration carefully.

## 3. A simplified theoretical model of coplanar interdigital electroadhesives

### 3.1. Understanding the coplanar interdigital capacitance

The interdigitated electrode geometry (see figure 3(a)) is a comb like periodic symmetric pattern and is the most preferred electroadhesive geometry. Detailed electric field lines of an interdigitated electroadhesive system can be seen in figures 3(b) and (c).

Since the length of the electrodes is much larger than their widths and thicknesses, and the electroadhesive pad area is much larger than the gap between the electrodes and the substrate surfaces, all the related fringing fields,  $E_l$ , resulted from edge/boundary effects, can be ignored. Although  $E_2$ , fields between electrodes due to electrode thickness, can induce relatively large attractive forces between the comb fingers, these forces on both sides of comb electrodes will cancel each other out. Also, due to  $E_2$  and because the electrodes are

deposited within the dielectrics, the electrodes will not touch each other. In addition, the effects between adjacent or overlapping fields are assumed to be neglected. As a consequence of these considerations, only the fields between the electrodes and the substrate,  $E_3$  and the fields between the coplanar electrode surfaces,  $E_4$  (which travel from the positive electrodes, penetrating the dielectric material and the substrate, to the negative electrodes), lead to the attractive forces within the interdigitated electroadhesive system.  $E_3$  is negligible compared with  $E_4$ . Therefore, only the half side closest to the wall substrate of  $E_4$  contributes primarily to the attractive forces between the pad and the substrate. Based on figures 3(a)–(c), we can create the equivalent circuit for the coplanar interdigitated capacitance presented in figure 3(d), where  $C_1$  and  $C_3$  are coplanar capacitances based on  $E_4$ , and  $C_2$  can be regarded as the normal parallel capacitance between electrodes because of  $E_2$ . Based on the assumptions and simplification made above, the electroadhesive forces between the pad and the substrate only depend on  $C_1$ , a parallel connection of pairs of coplanar capacitance units.

Various methods have been investigated to compute the coplanar capacitance within the interdigitated electroadhesive system, including the continuum model, finite element calculations, non-dimensionalized plot of capacitances, approximating expressions, and conformal mapping methods [20]. The conformal mapping method can transform a complex and coplanar geometry into a simple parallel circumstance and has been one of the most frequently used methods [40]. The existing approximate expressions were only applied on insulating substrates [41]. A theoretical model that is computationally easier and can be used for both conductive and non-conductive substrates is thus necessitated.

### 3.2. Optimization modelling of coplanar interdigital electroadhesives

The dimensions of the electrode width and space between electrodes has been assumed to be larger than 1 mm in this paper as the dielectric strength may change when the space between electrodes is smaller than 1 mm and no longer hold the rule, denoted by

$$s = \frac{U_{\max}}{\gamma}, \quad (10)$$

where  $\gamma$  is the dielectric strength and  $U_{\max}$  is the maximum voltage can be applied based on the minimum space between electrodes,  $s$ .

In order to derive the theoretical model, other assumptions have also been made in this paper. These assumptions are:

- the substrate thickness is infinite,
- no free charge exists in the electroadhesive system except on the electrodes,
- the charge distribution along the electrode is uniform thus the electric field distribution is uniform,
- the electric fields are continuous,
- the dielectric materials involved in the electroadhesive system are homogenous, linear, and isotropic,

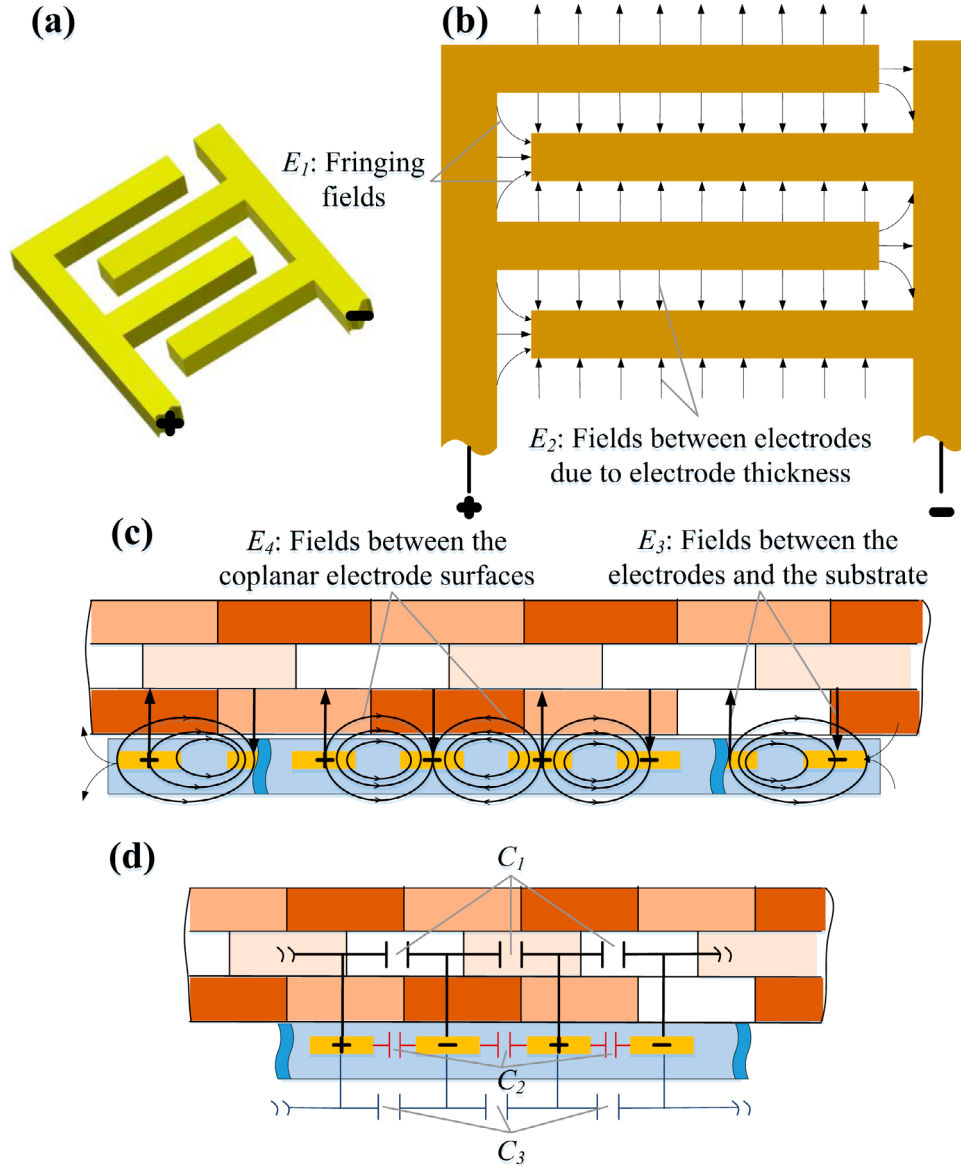


**Figure 3.** Electric fields and capacitances in the interdigitated electroadhesive system: (a) is the interdigitated electrodes in 3D, (b) is the top view of the interdigital electrodes, (c) is the cross-sectional view of the interdigital electroadhesive pad attached on a wall substrate, and (d) is the equivalent circuit for the coplanar interdigital capacitance.

- the pad is rigid and the contacting surfaces are completely flat, so no air gap exists between the pad and the substrate,
- the electrode thickness is negligible,
- the environment is stable,
- the edge effects are ignored as the length of electrodes or the pad area is assumed to be much larger than electrode widths and spaces between electrodes,
- and DC high voltage with dual polarity is used.

Please note that, as aforementioned, it is impossible to have an accurate analytical model that can predict the theoretical electroadhesive forces. Assumptions have to be made to derive a simplified theoretical electroadhesion model. Based on the assumptions above that the materials used in the electroadhesive system are homogenous, linear, and isotropic, the Gauss theorem can be applied. Theoretically the electric field lines should be distributed elliptically. Here, the electric field

ellipse lines are simplified into concentric lines to avoid conducting the curve integral of an ellipse mathematically. Since it has been assumed that the electric fields are uniformly distributed along the electrode length direction, the 3D problem can be transformed into a 2D one by taking the cross-section of the electrode panel into consideration, which can be seen in figure 4.

Since it has been assumed that there is no free charge in the space except the charges on the electrodes, the Laplace equation can then be applied. Therefore, under the polar coordinate condition, the equation is as follows

$$\Delta U = \frac{\partial^2 U}{\partial r^2} + \frac{1}{r} \frac{\partial U}{\partial r} + \frac{1}{r^2} \frac{\partial^2 U}{\partial \theta^2}. \quad (11)$$

Any radial plane that goes through the center can be regarded as equipotential planes and the electric field direction of every

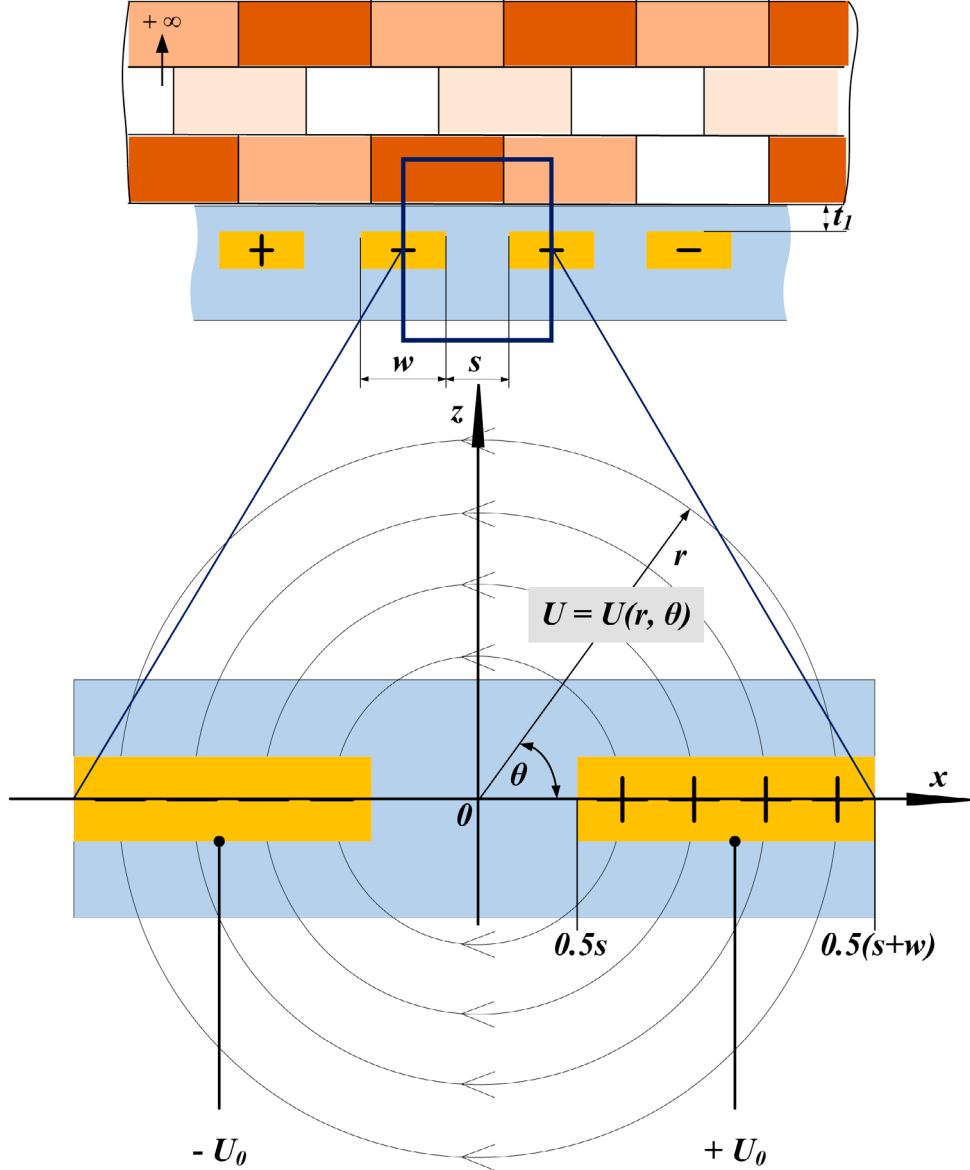


**Figure 4.** Simplified electric field distributions within the selected coplanar electrodes, where  $s$  is the space between electrodes,  $w$  is the electrode width,  $t_1$  is the dielectric thickness,  $r$  is the radius of the concentric electric field,  $\theta$  is the angle between the radius plane and electrode plane radius  $r$ , and  $U_0$  is the applied voltage on the electrodes.

point on these planes is perpendicular to these equipotential planes. The electric potential of any point in this system,  $U(r, \theta)$ , is a function of only  $\theta$ , giving

$$\frac{\partial^2 U}{\partial r^2} = \frac{1}{r} \frac{\partial U}{\partial r} = 0. \quad (12)$$

Hence, by substituting equation (12) into equation (11), the equation becomes

$$\frac{1}{r^2} \frac{\partial^2 U}{\partial \theta^2} = 0. \quad (13)$$

Considering the initial condition

$$\begin{cases} U(\theta = 0) = U_0 \\ U(\theta = \pi) = -U_0 \end{cases} \quad (14)$$

The electric potential in the system can be expressed as

$$U = U_0 - \frac{2U_0\theta}{\pi}. \quad (15)$$

Based on the Maxwell equation, the electric field is the gradient of the potential field

$$E = -\nabla U = \frac{2U_0}{\pi r}. \quad (16)$$

Based on Gauss' theorem, the charge density along the electrode surface is given as

$$\sigma = \epsilon_0 \epsilon_{\text{eff}} E = \epsilon_0 \epsilon_{\text{eff}} \frac{2U_0}{\pi r}, \quad (17)$$

where  $\epsilon_{\text{eff}}$  is the effective permittivity between the coplanar electrodes.

Since the thickness of the electrodes is negligible, all the charges are distributed along the surface of the electrodes, i.e.

the horizontal axis. It is then possible to obtain all the charges on the electrodes by integrating the charge density along the horizontal axis, giving

$$Q = \int_{0.5s}^{0.5(w+s)} \sigma dS = L \int_{0.5s}^{0.5(w+s)} \sigma dx = \frac{2LU_0\epsilon_0\epsilon_{eff}}{\pi} \ln\left(1 + \frac{w}{s}\right). \quad (18)$$

According to the definition of capacitance,

$$C_l = \frac{Q}{U} = \frac{Q}{2U_0} = \frac{L\epsilon_0\epsilon_{eff}}{\pi} \ln\left(1 + \frac{w}{s}\right). \quad (19)$$

The total capacitance of an interdigitated electroadhesive pad with  $N$  pair of fingers, based on (19), is

$$C_e = (2N - 1)C_l = \frac{(2N - 1)L\epsilon_0\epsilon_{eff}}{\pi} \ln\left(1 + \frac{w}{s}\right). \quad (20)$$

Since the selected coplanar unit area of the interdigitated electroadhesive is  $S = \frac{1}{2}L(w + s)$ , by substituting (19) into (2), the electrostatic attraction force per unit area can be the following equation

$$f_z = -\frac{8\epsilon_0\epsilon_{eff}^2 U_0^2}{\pi^2(w + s)^2} \left[ \ln\left(1 + \frac{w}{s}\right) \right]^2. \quad (21)$$

The problem of obtaining the maximum attraction force per unit area can be converted to a variable-constrained non-linear optimization problem based on (21). For the purpose of this research, the MATLAB function ‘fminsearchbnd()’ has been used. The objective function of the proposed optimization model and its constraints can be given as

$$\begin{aligned} \min_{x \rightarrow s.t. G(x) \leq 0} \{f(x)\} &= -\frac{8\epsilon_0\epsilon_{eff}^2 x_1^2}{\pi^2(x_2 + x_3)^2} \left[ \ln\left(1 + \frac{x_2}{x_3}\right) \right]^2 \\ x \rightarrow s.t. \quad &\begin{cases} -x_1 < 0 \\ x_1 \leq \min(U_{1\max}, U_{2\max}) \\ -x_2 \leq -1 \\ x_2 \leq l_1 \\ x_3 \leq l_2 \\ -x_3 \leq -x_3 \min \\ x_3 \min = \frac{x_1}{\gamma_1} \\ x_4 \leq l_3 \\ -x_4 \leq -x_4 \ min \\ x_4 \ min = \frac{x_1}{\gamma_2} \\ x_5 = \epsilon_{r1} \\ x_6 = \epsilon_{r2} \end{cases}, \end{aligned} \quad (22)$$

where  $x_1$  is the applied voltage,  $x_2$  is the width of electrodes and smaller than a designated value  $l_1$ ,  $x_3$  is the space between electrodes and smaller than a designated value  $l_2$ ,  $x_4$  is the thickness of the dielectric film and is smaller than a designated value  $l_3$ ,  $x_5$  is the permittivity of the dielectric film,  $x_6$  is permittivity of the substrate,  $\gamma_1$  is the dielectric strength of the dielectrics between the electrodes,  $\gamma_2$  the dielectric strength of the dielectrics covering the electrodes, and  $U_{i\max}$  is the maximum voltage that can be applied ( $i = 1, 2$ ).

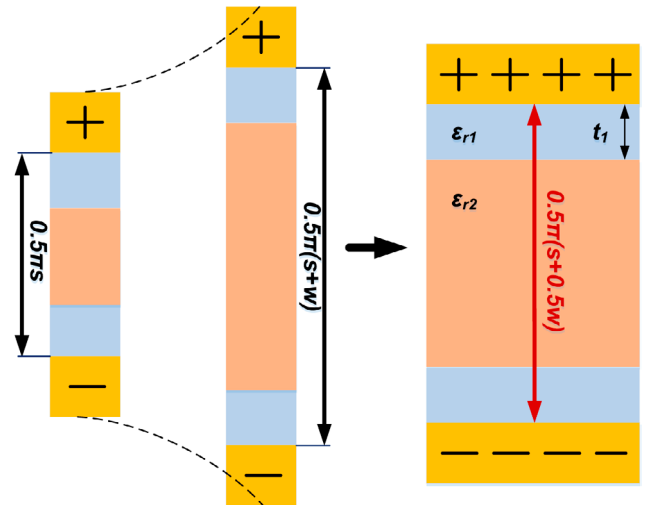


**Figure 5.** Simplified method for effective permittivity calculation.

When attaching the pad on conductive substrates, the effective permittivity can approximately be given by

$$\epsilon_{eff1} = \frac{\pi\epsilon_{r1}(s + 0.5w)}{t_1}. \quad (23)$$

When attaching the pad on insulating substrates, the effective permittivity can approximately be given by

$$\epsilon_{eff2} = \frac{\pi\epsilon_{r1}\epsilon_{r2}(s + 0.5w)}{4\epsilon_{r2}t_1 + \epsilon_{r1}[\pi(s + 0.5w) - 2t_1]}, \quad (24)$$

where  $\epsilon_{r1}$  is the relative permittivity of the dielectric layer,  $\epsilon_{r2}$  is the relative permittivity of the substrate, and  $t_1$  is the thickness of the dielectric layer.

The effective permittivity in the equations (23) and (24) was derived using classical equations on parallel capacitors, such as equation (1). The circular coplanar fields were simplified into straight fields from the positive electrodes, via the dielectric and substrate layers, to the negative electrodes. The average distance between the positive and negative electrodes was simplified as  $0.5\pi(s + 0.5w)$  (see figure 5). This has been inspired by the work published by Mamishev *et al* [20].

### 3.3. A worked example

For non-conductive substrates, the following assumptions were made:  $\gamma_1 = \gamma_2 = 60000 \text{ V mm}^{-1}$ ,  $1 \leq x_1 \leq \min(U_{1\max}, U_{2\max}) = 6000 \text{ V}$ ,  $1 \leq x_2 \leq 10 \text{ mm}$ ,  $1 \leq x_3 \leq 10 \text{ mm}$ ,  $0.1 \leq x_4 \leq 10 \text{ mm}$ ,  $2 \leq x_5 \leq 10$ , and  $2 \leq x_6 \leq 10$ . By using the MATLAB function fminsearchbnd(), the maximum attraction force per unit area on non-conductive substrates is  $0.0033 \text{ N mm}^{-2}$  (or  $3.3 \text{ kPa}$ ) under the condition of  $x_1 = 6000 \text{ V}$ ,  $x_2 = 1.79 \text{ mm}$ ,  $x_3 = 1 \text{ mm}$ ,  $x_4 = 0.1 \text{ mm}$ ,  $x_5 = 10$ , and  $x_6 = 10$ . The relationship between  $f_z$  and  $x_1$ ,  $x_2$ ,  $x_3$ ,  $x_4$ ,  $x_5$ , and  $x_6$  can be seen from figures 6(a)–(f) respectively.

From the results, it can be concluded that there is an optimum electrode width of  $1.79 \text{ mm}$  to achieve the maximum attraction force per unit area when attaching the pad on non-conductive substrates where the space between the electrodes has been fixed at  $1 \text{ mm}$  (optimum width/space ratio of  $1.79$ ). Also, the smaller the space between electrodes and

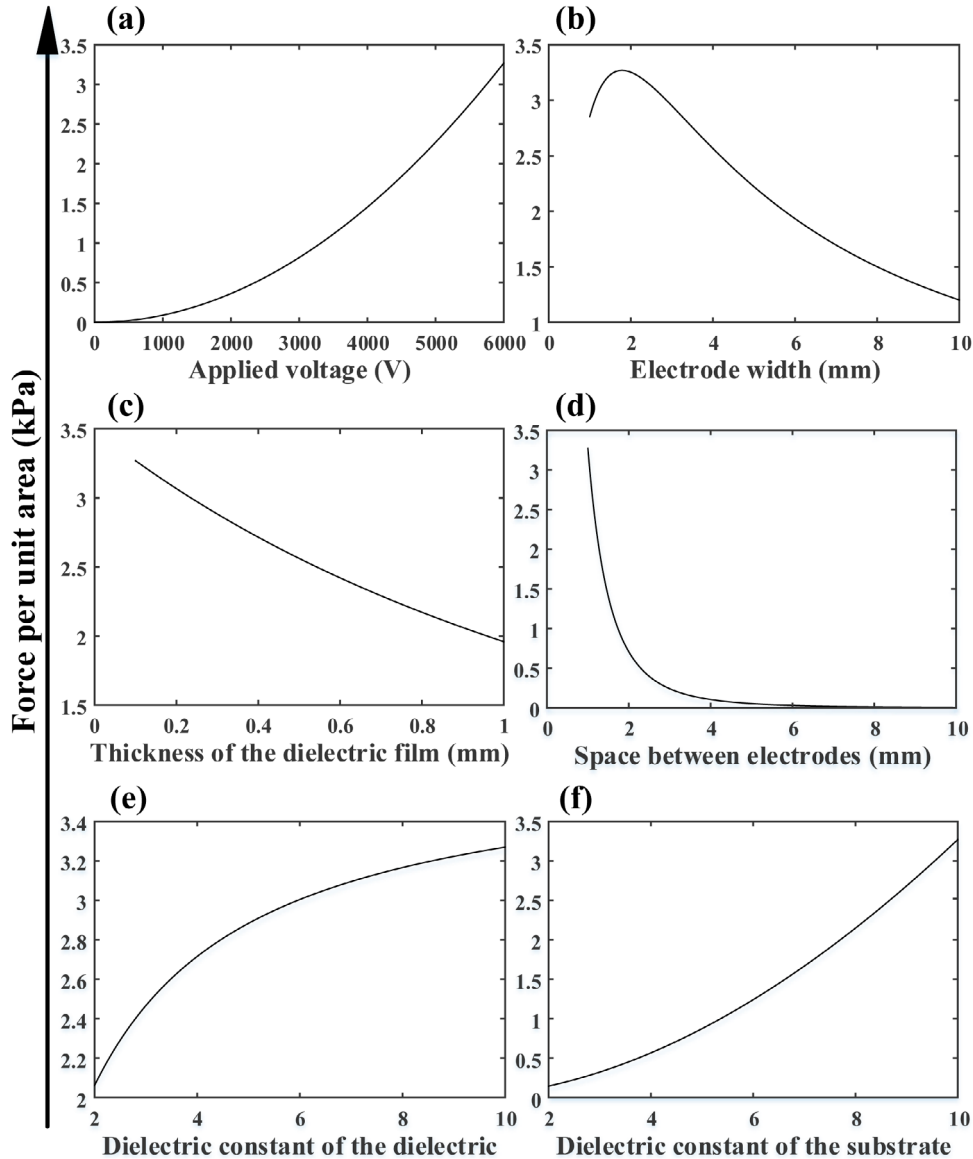


**Figure 6.** The theoretical relationship between force per unit area obtainable on nonconductive substrates and (a) applied voltage, (b) electrode width, (c) space between electrodes, (d) thickness of the dielectric, (e) dielectric constant of the dielectric, and (f) dielectric constant of the substrate.

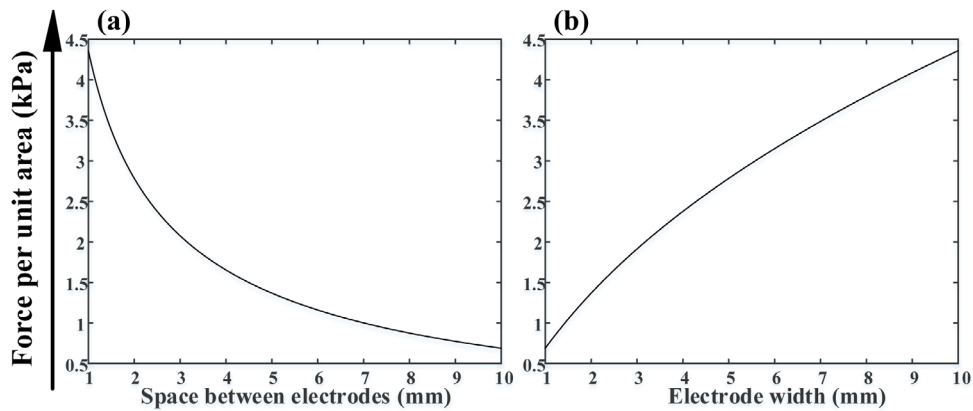


**Figure 7.** The theoretical relationship between force per unit area and (a) space between electrodes and (b) electrode width on conductive substrates.

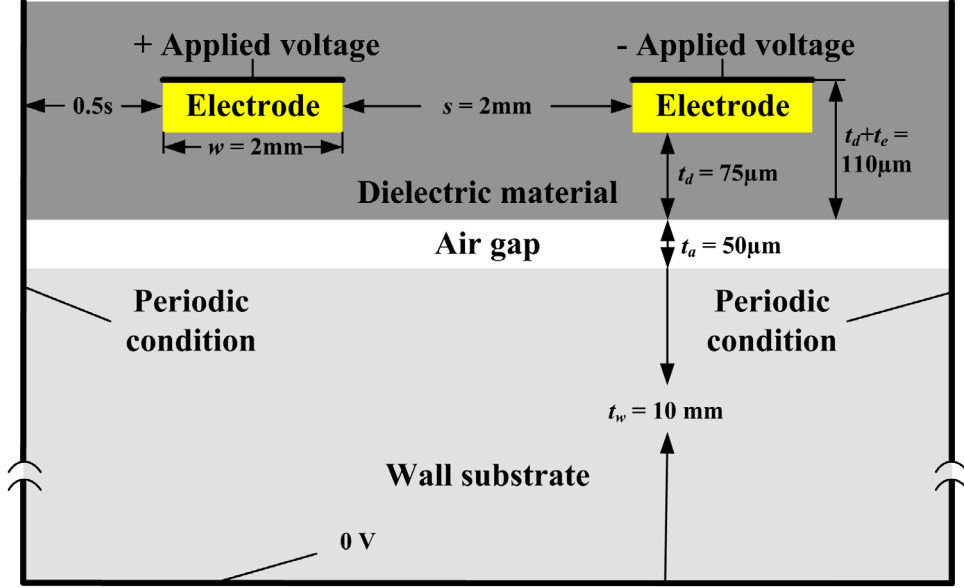


**Figure 8.** 2D electrostatic simulation model.  $w$  denotes the electrode width (pre-set as 2 mm),  $s$  denotes the space between electrodes (pre-set as 2 mm),  $t_d$  denotes the thickness of the dielectric layer (pre-set as 0.075 mm),  $t_e$  denotes the thickness of the copper electrodes (pre-set as 0.035 mm),  $t_a$  denotes the thickness of the air gap layer (pre-set as 0.05 mm), and  $t_w$  denotes the thickness of the glass substrate (pre-set as 10 mm). The dielectric constant of the dielectric material and glass substrate have been pre-set as 11.7 and 4.2 respectively. The applied voltage has been pre-set as 6000 V. The bottom of the wall substrate has been grounded and the potential has been set to 0 V. Since interdigital electroadhesive pads usually have periodical electrode arrays, periodic conditions have been applied.

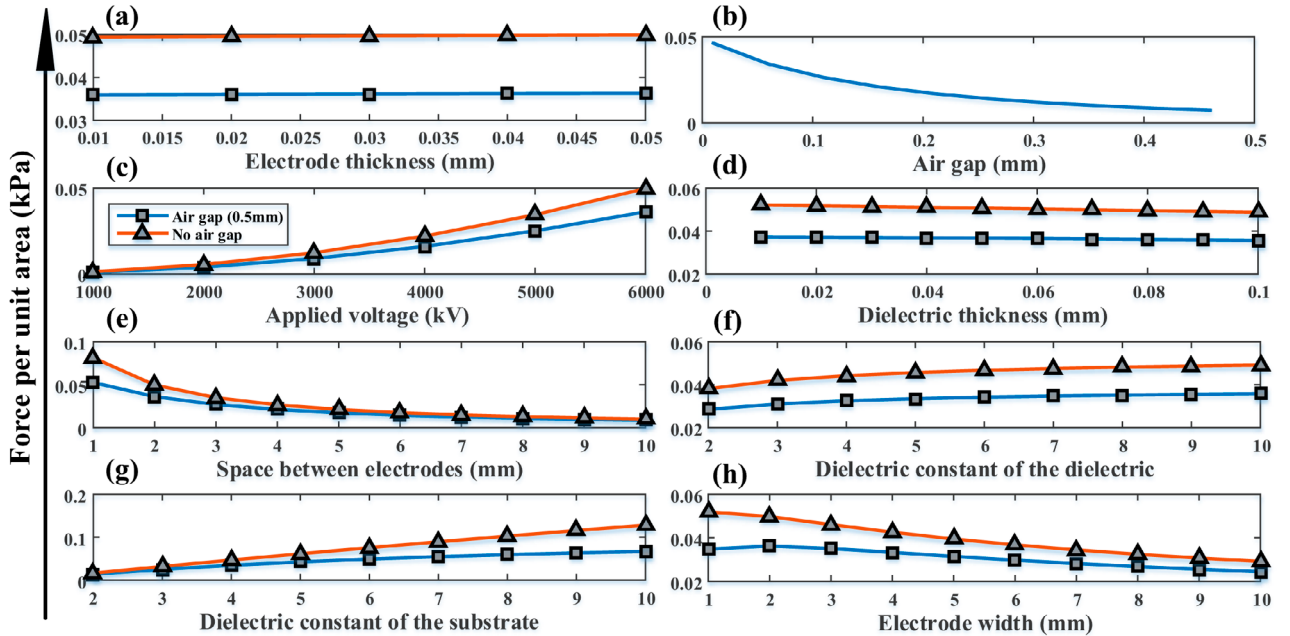


**Figure 9.** The relationship between force per unit area obtainable on non-conductive substrates and (a) electrode thickness, (b) air gap, (c) applied voltage, (d) thickness of the dielectric, (e) space between electrodes, (f) dielectric constant of the dielectric, (g) dielectric constant of the substrate and (h) electrode width based on COMSOL simulation.

the dielectric thickness, and the larger the permittivity of the dielectric film and the substrate, the larger the attractive forces obtainable. This is similar to the results shown in the work by Liu *et al* [24], Mao *et al* [25], and Cao *et al* [30].

For conductive substrates, the same parameter range as per the non-conductive case has been assumed. The space between electrodes should be as small as possible, as can

be seen from figure 7(a). However, a slightly different trend can be seen compared to the results from figure 6(c), manifesting that the change of space between electrodes is less sensitive to conductive substrates. It is obvious from figure 7(b) that the electrode width should be as large as possible to generate larger effective pad area thus larger force per unit area.

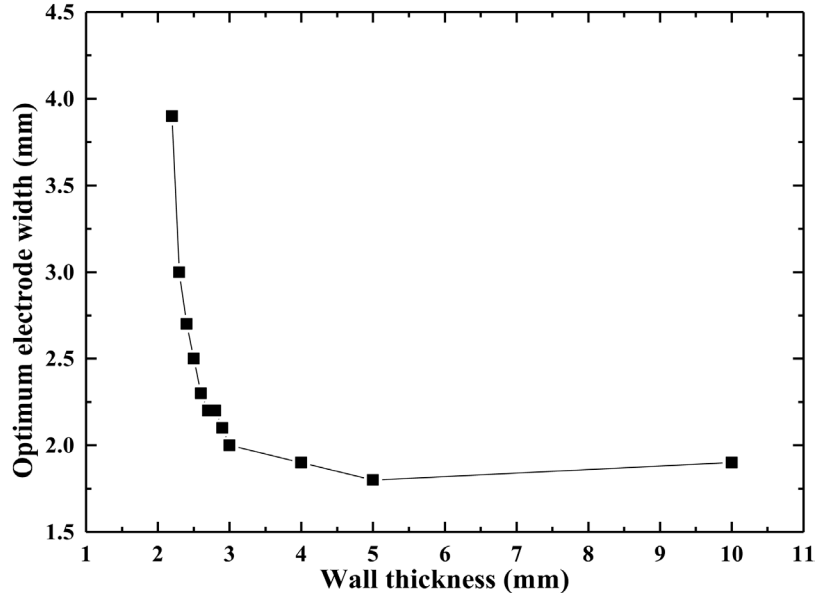


**Figure 10.** The relationship between wall thicknesses and optimum electrode widths for the 2D electrostatic simulation model with an air gap.

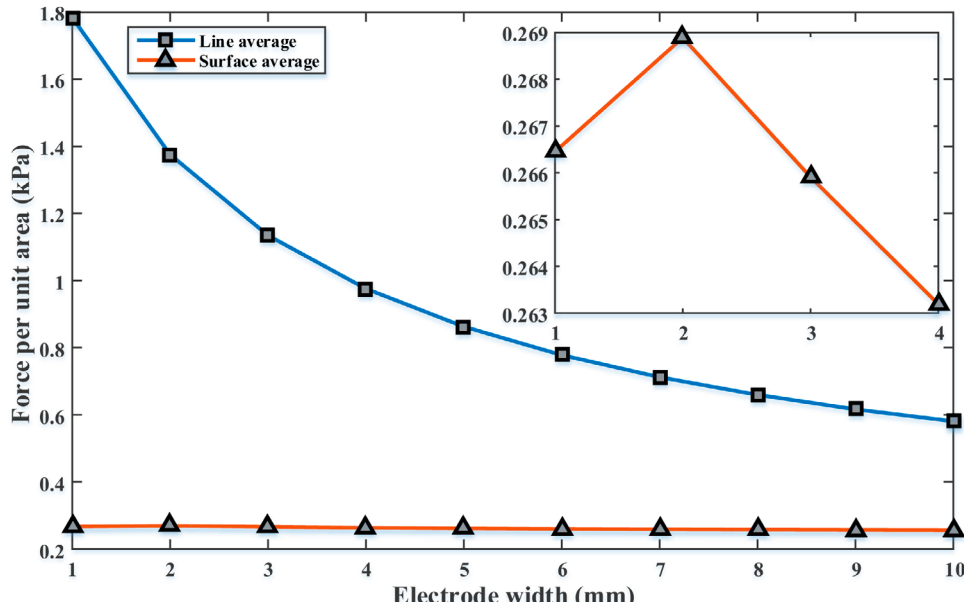


**Figure 11.** The difference between the line average method and the surface average method.

#### 4. 2D electrostatic simulation

A 2D electrostatic simulation based on COMSOL Multiphysics has been conducted to further support the results obtained from figure 5. The diagram of the 2D model can be seen in figure 8, where a non-conductive substrate such as a glass has been considered.

It can be seen from figure 9(a) that the electrode thickness has little effect on the electroadhesive forces obtainable. This supports the aforementioned assumption that it is reasonable to neglect the thickness of electrodes. It can be concluded from figure 9(b) that the smaller the air gap the larger the forces obtainable. Also, from figures 9(c)–(g), the result of the 2D model with an air gap and without has similar trends but the forces without an air gap are larger than with an air gap.

However, although the forces without an air gap are larger than with an air gap, a slightly different trend as be seen in figure 9(h).

For the simulation model without an air gap, the results have shown that

- for thinner wall substrates, where the thickness is  $\leq 1.7$  mm, the larger the electrode width, the larger the forces obtainable;
- for thicker wall substrates, where the thickness is  $\geq 2.2$  mm, the smaller the electrode width, the larger the forces obtainable;
- for wall substrates with thicknesses of  $1.8 \leq x_6 \leq 2.2$  mm, the optimum electrode widths of approximately 2.7 mm, 2.3 mm, 1.6 mm, and 1.9 mm can be found.

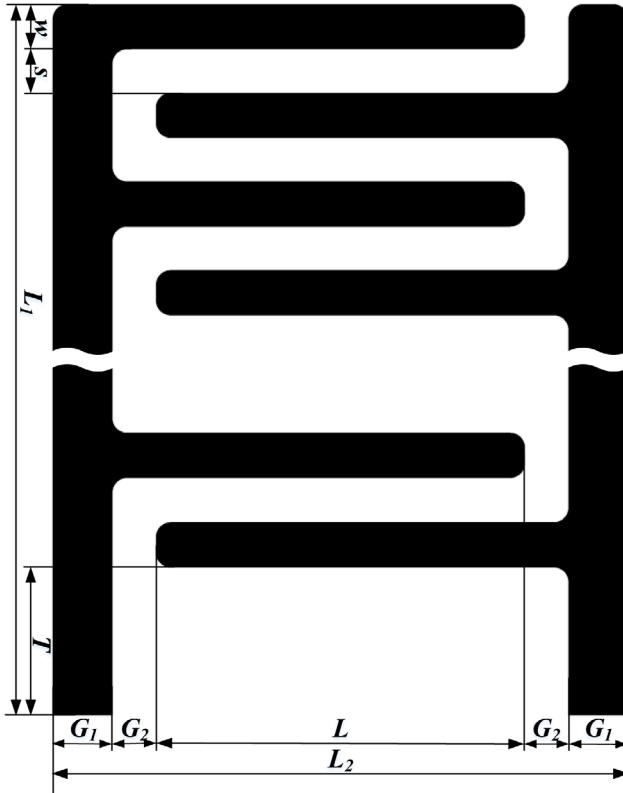


**Figure 12.** Interdigital coplanar electroadhesive pad design.

For the 2D electrostatic simulation model with an air gap, the results have shown that

- for thinner wall substrates, where the thickness is  $\leq 2.1$  mm, the larger the electrode width, the larger the forces obtainable;
- for thicker wall substrates, where the thickness is  $\geq 2.2$  mm, an optimum electrode width of approximately 2 mm can be found. Specifically, optimum electrode widths of 3.9 mm, 3 mm, 2.7 mm, 2.5 mm, 2.3 mm, 2.2 mm, 2.2 mm, 2.1 mm, 2 mm, 1.9 mm, 1.8 mm, and 1.9 mm were found when the wall thicknesses were 2.2 mm, 2.3 mm, 2.4 mm, 2.5 mm, 2.6 mm, 2.7 mm, 2.8 mm, 2.9 mm, 3 mm, 4 mm, 5 mm, and 10 mm respectively, as shown in figure 10.

It has to be noted that all the above simulation results have been based on considering the polarization of the whole substrate, i.e. the surface average of the whole substrate. If only the interfacial effect is considered, i.e. the line average of the contacting surface between the pad and the substrate, the smaller the electrode width, the larger the forces obtainable regardless of the thickness of the wall substrate. This agrees with most published results. The results shown in figure 11 have been based on a wall thickness of 2 mm. Also, the difference in the electroadhesive forces obtainable has been relatively small when changing the electrode width from 1 to 3 mm in all cases. Although there is an optimum width/space ratio of around 2 mm, the difference has been within 5% in the forces obtainable from electrode widths of 1 mm–3 mm.

**Table 1.** Geometric information of the pads for the experimental verification.

Electrode width (mm)	Electrode space (mm)
0.9	1
1.9	1
3.8	1
5.3	1
9.6	1
4	9.3
4	6.8
4	5
4	3.8
4	2.9

From the simulation results, on non-conductive substrate materials, in order to have more boundaries, it is advisable to have smaller electrode widths. Please note that all the above results have been based on the fact that the space between the electrodes has been fixed at 1 mm.

## 5. Experimental validation

### 5.1. Electroadhesive pad design and manufacture

The pads have been designed using Solidworks (see figure 12) and based on the following two equations

$$L_1 = T + (2N - 1)(w + s) + w, \quad (25)$$

and

$$L_2 = 2(G_1 + G_2) + L, \quad (26)$$

where  $L_1$  is the total length of the pad,  $L_2$  is the total width of the pad,  $L$  is the electrode overlap length,  $G_1$  is the width of electrode connection,  $G_2$  is the space between connection line and comb fingers,  $w$  is the electrode width,  $s$  is the space between electrodes,  $N$  (integral) is the number of electrode pairs, and  $T$  is the tail that can be used for the connection to the high voltage supply.

It is clear that the dielectric thickness of the dielectric layer should be as small as possible, only the electrode width and space between electrodes have been varied. In order to make all the pad designs the same effective pad area, the parameters have been therefore set as  $T = 40$  mm,  $L_1 = 270$  mm,  $L_2 = 170$  mm,  $L = 150$  mm, and  $G_1 = G_2 = 5$  mm.

For the investigation into the relationship between electrode widths and the obtainable electroadhesive force, all the other geometrical parameters have been maintained ( $s = 1$  mm). Five pads that have different electrode widths have been generated. For the investigation into the relationship between the space between electrodes and the electroadhesive forces obtainable, all the other geometrical parameters have been maintained ( $w = 4$  mm). Five pads that have different spaces between electrodes have been generated. The geometric information of the ten pads can be seen in table 1. The designed pads have been then professionally manufactured using the procedures presented in figure 13.

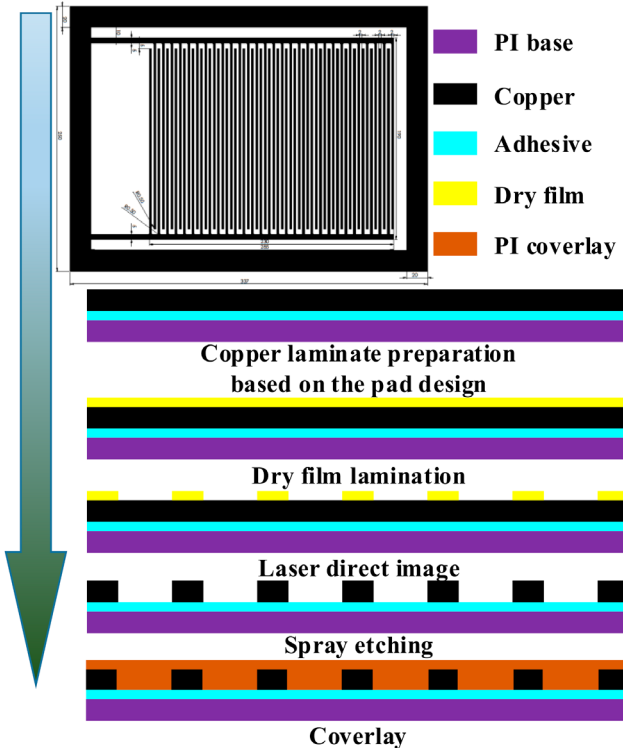


**Figure 13.** Electroadhesive pad manufacture procedure. The copper electrode thickness has been set to  $18\ \mu\text{m}$ , the polyimide base (PI dielectric constant: 3.2) thickness has been set to  $12.5\ \mu\text{m}$  including an unknown thickness of adhesive and the PI overlay has been a combination of a  $12.5\ \mu\text{m}$  PI (dielectric constant: 3.8) with a  $15\ \mu\text{m}$  adhesive. The copper area outside of the interdigitated pattern has been for supporting the pad flat enough during the overlaying process. Only the interdigitated pattern part of the design has been used for the electroadhesive force testing. The effective pad area has been designed as  $170\ \text{mm} \times 230\ \text{mm}$ .

### 5.2. Electroadhesive force measurement platform and procedure

A bespoke mechatronic and reconfigurable electroadhesive force measurement platform has been used to obtain the normal electroadhesive forces between the electroadhesive pad and substrates. Please note that all the experimental results in the literature have shown that the shear electroadhesive forces are larger than that of in normal when measuring the shear and normal forces on the same substrate. Most previous recorded results have not presented the inclusion of suction forces (if not tested in vacuum) and van der Waals forces between the pad and the substrate in detail after the application of high voltages. The inclusion of suction forces due to the air gap and van der Waals forces due to the intimate contact can be seen in figure 14(a). The actual normal forces the sensor will obtain can therefore be expressed as

$$F_{\text{normal}} = F_{\text{ea}} + F_{\text{suction}} + F_{\text{van}}, \quad (27)$$

where  $F_{\text{ea}}$  is the normal electroadhesive forces,  $F_{\text{suction}}$  is the suction forces between the pad and the substrate, and  $F_{\text{van}}$  is the van der Waals forces.

When a shear force is applied on the pad, restriction forces occur, as shown in figure 14(b) [15], which may be the main reason that the recorded shear forces are stronger than the

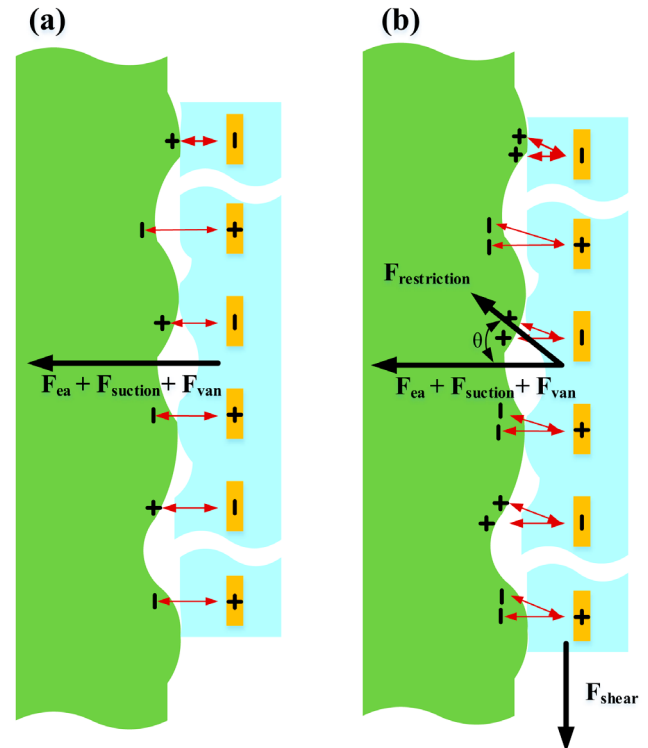


**Figure 14.** The force analysis between the electroadhesive pad and the substrate when: (a) no shear force is applied and (b) a shear force is applied on the pad (note that the weight of the pad is neglected).

normal forces. Assuming that there is an angle,  $\theta$ , as illustrated in figure 14(b), between the forces in normal and the restriction forces, the recorded shear electroadhesive forces can then be expressed as:

$$F_{\text{shear}} = \mu(F_{\text{ea}} + F_{\text{suction}} + F_{\text{restriction}} \cos \theta) + F_{\text{restriction}} \sin \theta. \quad (28)$$

It is therefore inappropriate to derive the normal electroadhesive forces by the division of the measured shear forces and friction coefficients although this has been used by some researchers [9, 10, 26]. As it is difficult to quantify the restriction force, suction force, and van der Waals forces, it is therefore also inappropriate to use the measured shear forces to validate the models considering normal electroadhesive forces. The system diagram of the advanced electroadhesive force measurement setup can be seen in figure 15(a), where a 6-axis ATI Gamma Force/Torque ( $F/T$ ) sensor was used to record the normal electroadhesive forces. The communication between the  $F/T$  sensor and the computer has been through a Netbox via an Ethernet cable and the data has been selected to be sampled at 152 Hz. The linear rail can achieve horizontal movement using a servo motor with an encoder driven by a Kollmorgen motor driver connected with a CompactRIO. This has allowed almost real time control of the linear rail via a Xilinx FPGA which has been designed to communicate with the computer via Ethernet. The smallest movement of the linear rail that the encoder can detect has been approximately  $0.8\ \mu\text{m}$ . The electroadhesive pad has been connected with two EMCO high voltage converters (HVCs) with  $(\pm)$   $0\text{--}10\text{kV}$  output and  $0\text{--}5\text{V}$  reference input. The reference input

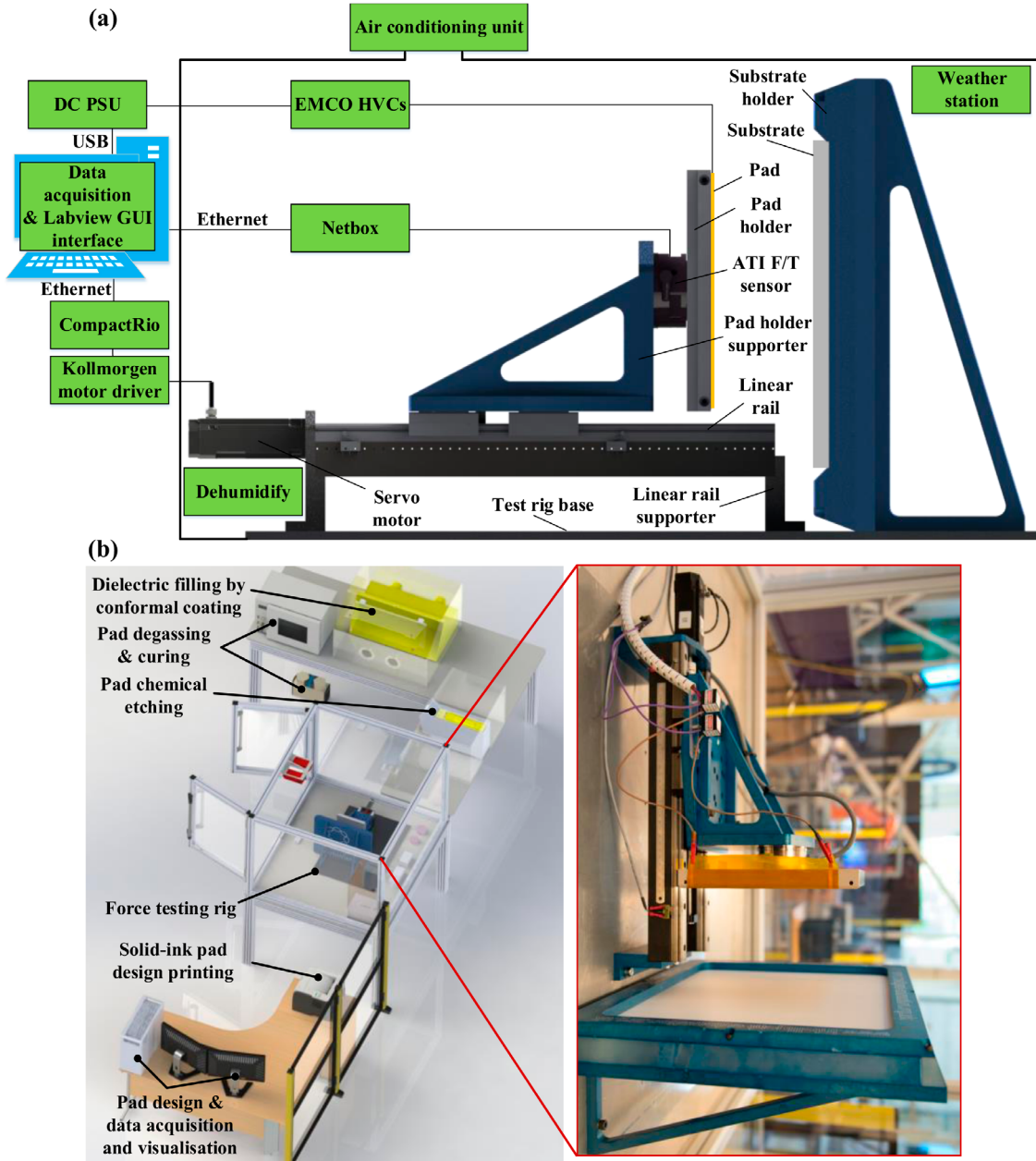


**Figure 15.** Electroadhesive force measurement platform: (a) system diagram and (b) physical setup.

has been from a direct current power supply unit (DC PSU), Instek GPD3303, which has been designed to communicate with the computer through via a USB. The physical normal electroadhesive force measurement platform can be seen in figure 15(b). A Labview interface has been developed for interactive control of the movement of the linear rail, changing the supply voltage, recording, and saving the electroadhesive force data. Please note that an electrical safety interlock system and safety screens have been applied in this advanced measurement platform.

The electroadhesive force measurement procedures can be seen in figure 16. The pad has been initially attached on the PEEK pad holder and the substrates have been clamped in the substrate holder. A  $30 \pm 1\text{ N}$  preload has been then applied on the substrates. The recording of the electroadhesive force has been then started by turning on the power supply, thus

providing power to the pad. The pad has been charged for 60s. After this, the pad has been pulled away by activating the servo motor. When the motor stopped, the data recording has been completed and the data has been exported as text files. These files have been further filtered and analyzed in MATLAB. The next experiment has been conducted after 540s. The start of this lag time has been at the commencement of the pulling away of the pad. The dwell time has been useful for residual charge dissipation. During the residual charge dissipation process, the pad has been grounded for 300s after each test. Also, the aluminium (Al) substrate has been grounded for 300s each time before the pad has been changed. A Simco-Ion electrostatic fieldmeter, mounted on Kanya frames, has been used to compare the surface charge value of the plate before applying the voltage and after the grounding. 300s have shown to be enough to obtain similar

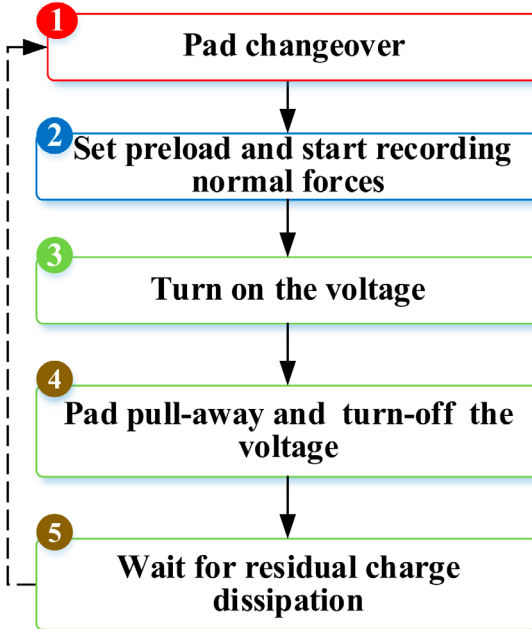


**Figure 16.** Electroadhesive force measurement procedure [19]. Reproduced with permission from [19]. Copyright 2016 IOP Publishing.

results within less than 5% difference. Also, each time after applying the preload, little difference has been observed after 30 s' stabilizing. A fixed experiment time of 10 min (540 s plus 60 s) for each test has been therefore set for this investigation. The motor pull-off velocity ( $0.1 \text{ mm s}^{-1}$ ) and pull-off acceleration ( $50 \text{ revs}^{-2}$ ), charge time (60 s) and discharge time (540 s) have been maintained at constant values when conducting the experiments for the 10 pads demonstrated in table 1. For each pad, six experiments have been repeated. The first data point for each pad has not been used for data analysis.

To date, little evidence has been found to systematically investigate the influence of environmental factors on the electroadhesive forces. Environmental factors affect and modify the dielectric properties of electroadhesive pads such as dielectric strength, permittivity, and resistivity. Also, they arouse electric discharges and dielectric degradation that causes the failure of the adhesion. Within the research laboratory where our fundamental research has been undertaken, the lab temperature has changed from 17 to 28 °C, relative humidity changed from 28 to 73% and air pressure changed from 996.3 to 1015.2 hPa between January and August 2015. Preliminary results have been obtained over a 5 d period when all variables have been maintained, as shown in table 2, except the temperature (20.8–21.5 °C), relative humidity (43–64%) and air pressure (993.8–1013 hPa). The electroadhesive pad used this test has been based a customized chemical etching and conformal coating. The PUC side (dielectric constant: 3.6) of the pad has been facing the substrate. The results can be seen in figure 17, where a nearly 200% relative difference in forces has been observed. The result shown in figure 17 is maybe the reason that hinders the current application of flexible electroadhesive solutions in ambient industrial environments where unstable and unpredictable forces may be achieved. In order to control the environment factors to validate the proposed model, a

**Table 2.** Controlled parameters for the force testing in the changing ambient environment.

Controlled parameters	Values
Applied voltage (kV)	2
Voltage polarity	Dual polarity ( $\pm$ )
Substrate material and thickness	12 mm toughened glass on a metal plate
Charge/discharge time (s)	90/510
Pad effective area	170 mm $\times$ 230 mm
Dielectric base material	Polyester (PET)
Dielectric base material thickness ( $\mu\text{m}$ )	23
Dielectric cover material	Polyurethane (PUC)
Dielectric cover material thickness ( $\mu\text{m}$ )	Approximately 20
Electrode space (mm)	5
Electrode width (mm)	4
Electrode material	Copper
Electrode thickness ( $\mu\text{m}$ )	20
Pad holder pull away velocity ( $\text{mm s}^{-1}$ )	0.1
Pad holder pull away acceleration ( $\text{revs}^{-2}$ )	50
Preload (air gap, N)	$30 \pm 1$

well-sealed chamber enclosing the force test rig has been used so that the testing can be free of contaminates/dusts. An air conditioning unit and a dehumidifier (see figure 13(a)) have been employed to maintain the temperature, humidity, and air pressure. The temperature has been maintained at  $25^\circ\text{C} \pm 0.2^\circ\text{C}$ , humidity at  $32\% \pm 2\%$ , and pressure at 1013 hPa  $\pm 1$  hPa, when testing the 10 pads mentioned in table 1.

### 5.3. Results

The electroadhesive forces have been recorded when the PI base side has been facing the substrates: a toughened glass or an Al plate. 2 kV has been applied on the pads. Before each test, the force with no voltage applied has been recorded to check the potential suction forces, van der Waals forces, and surface tension forces. For all the 10 pads, less than 0.05 N has been observed when no voltage has been applied. This means the forces recorded under a voltage are predominately the normal electroadhesive forces. The experimental results manifesting the relationship between the electroadhesive forces obtainable and the spaces between electrodes can be seen in figure 18. For both conductive substrates, such as the Al plate, and non-conductive substrates, such as the toughened glass, the smaller the space between electrodes, the larger the electroadhesive forces obtainable. This agrees with all the theoretical and simulation results.

The experimental results manifesting the relationship between the electroadhesive forces obtainable and the electrode widths can be seen in figure 19. For non-conductive substrates such as the toughened glass, there indeed is an optimum width/space ratio of approximately 1.9 mm.

There is, however, only an approximately 21% relative difference in the electroadhesive forces obtainable when changing the electrode width from 0.9 mm to 3.8 mm. For conductive substrates such as the Al plate, the width/space ratio should be as large as possible to have a larger effective pad area thus larger force per unit area obtainable. The difference

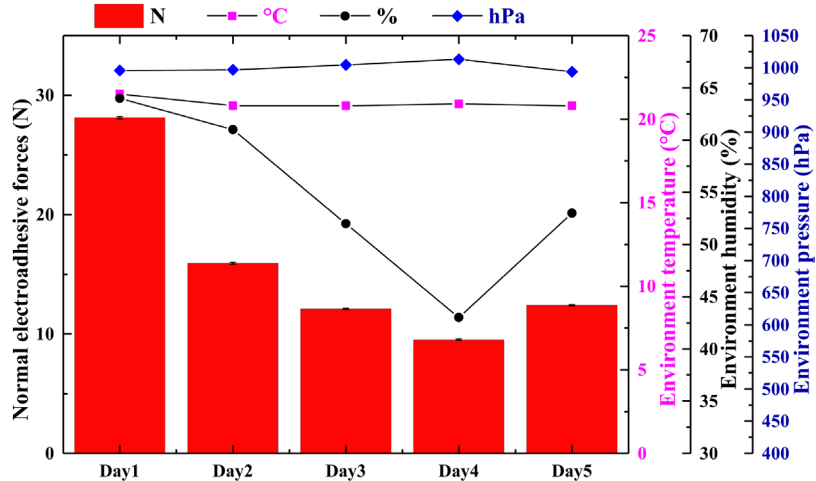


Figure 17. Electroadhesive forces measured in a 5 d period.

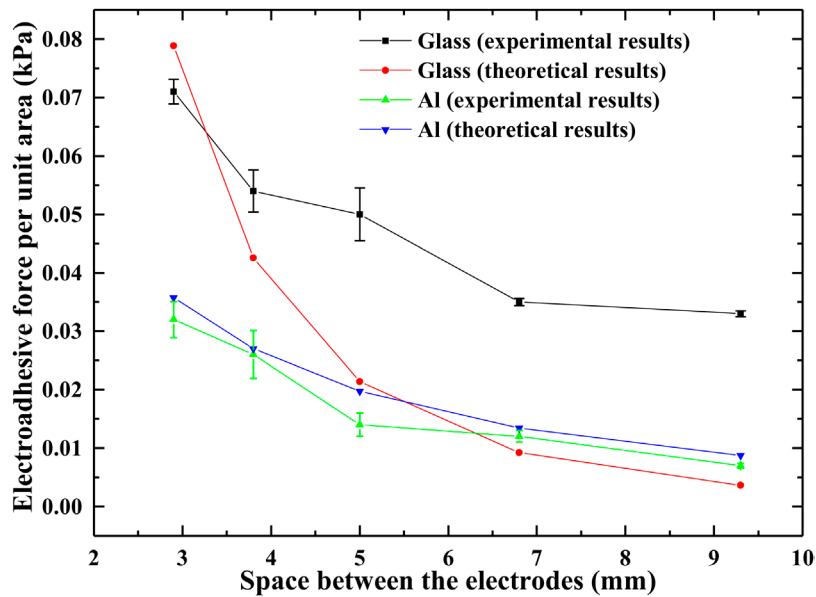


Figure 18. Experimental validation of the relationship between the electroadhesive forces obtainable and spaces between the electrodes and its comparison with the theoretical results.

between the theoretical and experimental results is relatively small, as compared in figures 18 and 19. Please note that, due to the simplified assumptions mentioned above, a factor has been used to multiply the measured forces in order to compare the theoretical and experimental results. The slight difference in the general trends may due to the fact that there is a layer of air between the pad and the substrate during the force testing.

## 6. Conclusion and future work

The work presented in this paper has focused upon the optimization modelling of interdigital electroadhesives and its experimental validation of the existence of an optimum width/space ratio based on a confident testing platform and procedure. The key findings from this work are that:

- The proposed 2D electrostatic simulation results have shown that the wall thickness and air gap have a large

bearing on the optimum widths achievable for non-conductive substrates. The consideration of only the interfacial electric fields and the electric fields within the whole substrate have generated a different result. If only the interfacial electric fields are considered, the smaller the electrode width, the larger the forces obtainable regardless of the effect of the wall thickness. If the electric fields within the whole substrate are considered, an optimum electrode width can always be found when the space between electrodes is fixed. This may be the reason why the existing simulation results have demonstrated different conclusions.

- The proposed simplified and computationally easier theoretical optimization modelling of coplanar interdigitated electroadhesives is promising for predicting the performance of an interdigitated electroadhesive actuator. The theoretical model have shown that there is an optimum electrode width/space between electrodes

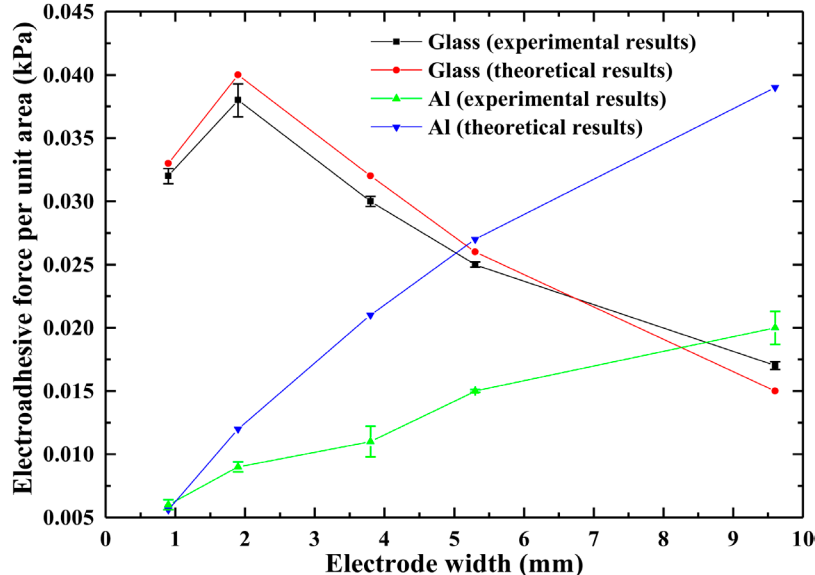


**Figure 19.** Experimental validation of the relationship between the electroadhesive forces obtainable and electrode widths and its comparison with the theoretical results.

ratio of approximately 1.8 for interdigital pads to achieve the maximum forces on non-conductive substrates. For conductive substrates, the width/space ratio should be as large as possible. This has been validated by the experimental results both on conductive substrates such as the Al plate and non-conductive substrates such as the glass. On the Al plate, the larger the electrode width, the larger the effective pad area, thus the larger the forces obtainable. On the glass plate, there is an optimum electrode width of approximately 1.9 mm when the space between the electrodes has been fixed at 1 mm (optimum width/space ratio of approximately 1.9).

- The electroadhesive force analysis proposed in figure 13 highlights the inappropriateness to derive the normal forces by the division of the measured normal forces and friction coefficients. The measured normal forces are therefore only useful for validating the normal force based models.
- The result demonstrated in figure 16 not only highlights the importance of controlling the environment when testing the pads to validate the models but also identifies the need for the investigation of environmentally stable electroadhesives.

The understanding and modelling of electroadhesion presented in this paper is useful for optimized electroadhesive end effector designs for electroadhesive based robotic material handling applications currently under investigation by the authors. Future work will contain a more comprehensive experimental validation work using more pads tested in vacuum to both validate the relationship between forces obtainable and other parameters and the obtained simulation results. A theoretical model including the thickness of the wall substrate and air layer will also be considered. A nearly quadratic relationship between the applied voltages and the electroadhesive forces obtainable can only be seen when the applied voltage is less than 6000V. The proposed model is

therefore limited to applied voltages smaller than 6000V. Future work will also therefore contain the investigation of a more comprehensive model considering voltages beyond 6000V. In addition, a systematic investigation into the relationship between the environmental factors and electroadhesive forces obtainable is needed, aiming not only to produce environmental stable electroadhesives but also a more accurate model considering environmental factors and minimising the number of aforesaid assumptions. These will further aid the design and implementation of optimized electroadhesive end effectors for future material handling applications.

## Acknowledgments

The authors acknowledge support from the EPSRC Centre for Innovative Manufacturing in Intelligent Automation, in undertaking this research work under grant reference number EP/IO33467/1.

## References

- [1] Krape R P 1968 Applications study of electroadhesive devices *NASA Contractor Report*: NASA CR-1211 National Aeronautics and Space Administration
- [2] Warning R W 1960 Electrostatic force employed to hold workpieces *Phys. Forces Electrostat. Appl.* **1** 17–27
- [3] Beasley G and Hankins W 1971 Development of electroadhesive devices for zero-g intraextravehicular activities *AIAA pp 71–853*
- [4] Leung B, Miller L, Goeser N and Gonzalez S 2015 Validation of electroadhesion as a docking method for spacecraft and satellite servicing *IEEE Aerospace Conf. (Big Sky, Montana, 7–14 March 2015)* pp 1–8
- [5] Wardly G 1973 Electrostatic wafer chuck for electron beam microfabrication *Rev. Sci. Instrum.* **44** 1506–9
- [6] Monkman G J, Taylor P M and Farnworth G J 1989 Principles of electroadhesion in clothing technology *Int. J. Clothing Sci. Technol.* **1** 14–20

- [7] Monkman G J 1995 Robot grippers for use with fibrous materials *Int. J. Robot. Res.* **14** 144–51
- [8] Zhang Z, Chestney J A and Sarhadi M 2001 Characterizing an electrostatic gripping device for the automated handling of non-rigid materials *Proc. Inst. Mech. Eng. B* **215** 21–36
- [9] Yamamoto A, Nakashim Y T and Higuchi T 2007 Wall climbing mechanisms using electrostatic attraction generated by flexible electrodes *Int. Symp. on Micro-NanoMechatronics and Human Science (Nagoya, 11–14 November 2007)* pp 389–94
- [10] Prahlad H, Pelrine R, Stanford S, Marlow J and Kornbluh R 2008 Electroadhesive robots-wall climbing robots enabled by a novel, robust, and electrically controllable adhesion technology *IEEE Int. Conf. on Robotics and Automation (Pasadena, 19–23 May 2008)* pp 3028–33
- [11] Seitz B, Goldberg B, Doshi N, Ozcan O, Christensen D, Hawkes E, Cutkosky M and Wood R 2014 Bio-inspired mechanisms for inclined locomotion in a legged insect-scale robot *IEEE Int. Conf. on Robotics and Biomimetics (Bali, 5–10 December 2014)* pp 791–6
- [12] Grabit Inc. <http://grabitinc.com/>
- [13] Guo J, Justham L, Jackson M and Parkin R 2015 A concept selection method for designing climbing robots *Key Eng. Mater.* **649** 22–9
- [14] Ruffatto D, Shah J and Spenko M 2014 Increasing the adhesion force of electrostatic adhesives using optimized electrode geometry and a novel manufacturing process *J. Electrostat.* **72** 147–55
- [15] Yatsuzuka K, Hatakeyama F, Asano K and Aonuma S 2000 Fundamental characteristics of electrostatic wafer chuck with insulating sealant *IEEE Trans. Ind. Appl.* **36** 510–6
- [16] Jeon J U and Higuchi T 1999 Electrostatic suspension of dielectrics *IEEE Trans. Ind. Electron.* **45** 938–46
- [17] Monkman G J 1987 Electrostatic techniques for fabric handling *MSc thesis* The University of Hull
- [18] Graule M, Chirarattananon P, Fuller S, Jafferis N, Ma K, Spenko M, Kornbluh R and Wood R 2016 Perching and takeoff of a robotic insect on overhangs using switchable electrostatic adhesion *Science* **352** 978–82
- [19] Guo J, Tailor M, Bamber T, Chamberlain M, Justham L and Jackson M 2016 Investigation of relationship between interfacial electroadhesive force and surface texture *J. Phys. D: Appl. Phys.* **49** 35303
- [20] Mamishev A, Sundara-Rajan K, Yang F, Du Y and Zahn M 2004 Interdigital sensors and transducers *Proc. IEEE* **92** 808–44
- [21] Asano K, Hatakeyama F and Yatsuzuka K 2002 Fundamental study of an electrostatic chuck for silicon wafer handling *IEEE Trans. Ind. Appl.* **38** 840–5
- [22] Mao J et al 2014 Modelling and simulation of electrostatic attraction force for climbing robots on the conductive wall material *IEEE Int. Conf. on Mechatronics and Automation (Tianjin, 3–6 August 2014)* pp 987–92
- [23] Liu R, Chen R, Shen H and Zhang R 2012 Wall climbing robot using electrostatic adhesion force generated by flexible interdigital electrodes *Int. J. Adv. Robot. Syst.* **10** 1–9
- [24] Liu R, Chen R and Shen H 2013 Modeling and analysis of electric field and electrostatic adhesion force generated by interdigital electrodes for wall climbing robots *IEEE Int. Conf. on Intelligent Robots and Systems (Tokyo, 3–7 November 2013)* pp 2327–32
- [25] Mao J, Qin L, Zhang W, Xie L and Wang Y 2015 Modeling and analysis of electrostatic adhesion force for climbing robot on dielectric wall materials *Eur. Phys. J. Appl. Phys.* **69** 11003
- [26] Monkman G 1997 An analysis of astrinctive prehension *Int. J. Robot. Res.* **16** 1–10
- [27] Tellez J P D, Krahn J and Menon C 2011 Characterization of electro-adhesives for robotic applications *IEEE Int. Conf. on Robotics and Biomimetics (Karon Beach, Phuket, 7–11 December 2011)* pp 1867–72
- [28] Germann J, Dommer M, Pericet-Camara R and Floreano D 2012 Active connection mechanism for soft modular robots *Adv. Robot.* **26** 785–98
- [29] Schubert B and Floreano D 2014 Stretchable electroadhesion for soft robots *IEEE/RSJ Int. Conf. on Intelligent Robots and Systems (Chicago, 14–18 September 2014)* pp 3933–8
- [30] Cao C, Sun X, Fang Y, Qin Q, Yu A and Feng X 2016 Theoretical model and design of electroadhesive pad with interdigitated electrodes *Mater. Des.* **89** 485–91
- [31] Ruffatto D, Shah J and Spenko M 2014 Improving controllable adhesion on both rough and smooth surfaces with a hybrid electrostatic/gecko-like adhesive *J. R. Soc. Interface* **11** 1–10
- [32] Koh K, Ramanathan K and Ponnambalam S 2011 Modeling and simulation of electrostatic adhesion for wall climbing robot *IEEE Int. Conf. on Robotics and Biomimetics (Karon Beach, Phuket, 7–11 December 2011)* pp 2031–6
- [33] Saberman V, Hojjat Y and Hasanzadeh H 2014 Study of parameters affecting the electrostatic attractions force *Int. J. Electr. Comput. Electron. Commun. Eng.* **8** 1628–31
- [34] Kao K 2004 *Dielectric Phenomena in Solids: with Emphasis on Physical Concepts of Electronic Processes* (San Diego, CA: Elsevier)
- [35] Qin S and McTeer A 2007 Wafer dependence of Johnsen–Rahbek type electrostatic chuck for semiconductor processes *J. Appl. Phys.* **104** 064901
- [36] Shim G and Sugai H 2008 Dechuck operation of Coulomb type and Johnsen–Rahbek type of electrostatic chuck used in plasma processing *Plasma Fusion Res.* **3** 051
- [37] ElectroGrip Co. [www.electrogrip.com/Egrif2013Support/faq2006no1.pdf](http://www.electrogrip.com/Egrif2013Support/faq2006no1.pdf)
- [38] Atkinson R 1969 A simple theory of the Johnsen–Rahbek effect *J. Phys. D: Appl. Phys.* **2** 325–32
- [39] Jin J, Higuchi T and Kanemoto M 1995 Electrostatic levitator for hard disk media *IEEE Trans. Ind. Electron.* **42** 467–73
- [40] Igreja R and Dias C 2011 Extension to the analytical model of the interdigital electrodes capacitance for a multi-layered structure *Sensors Actuators A* **172** 392–9
- [41] den Otter M 2002 Approximate expressions for the capacitance and electrostatic potential of interdigitated electrodes *Sensors Actuators A* **96** 140–4